TSHZ1-dependent gene regulation is essential for olfactory bulb development and olfaction

Daniela Ragancokova,[1] Elena Rocca,[1] Anne M.M. Oonk,[2,3] Herbert Schulz,[4] Elvira Rohde,[1] Jan Bednarsch,[5] Ilse Feenstra,[6] Ronald J.E. Pennings,[2,3] Hagen Wende,[1] and Alistair N. Garratt[1,7]

[1]Neuroscience Program, Max-Delbrück-Center for Molecular Medicine (MDC), Berlin, Germany. [2]Department of Otorhinolaryngology, Radboud University Nijmegen Medical Centre, Nijmegen, The Netherlands. [3]Donders Institute for Brain, Cognition and Behaviour, Radboud University Nijmegen, Nijmegen, The Netherlands. [4]Cardiovascular Program, MDC, Berlin, Germany. [5]Department of General, Visceral, and Transplantation Surgery, Charité University Hospital Berlin, Berlin, Germany. [6]Human Genetics, Hearing, and Genes, Radboud University Nijmegen Medical Centre, Nijmegen, The Netherlands. [7]Institute of Cell Biology and Neurobiology, Center for Anatomy, Charité University Hospital Berlin, Berlin, Germany.

The olfactory bulb (OB) receives odor information from the olfactory epithelium and relays this to the olfactory cortex. Using a mouse model, we found that development and maturation of OB interneurons depends on the zinc finger homeodomain factor teashirt zinc finger family member 1 (TSHZ1). In mice lacking TSHZ1, neuroblasts exhibited a normal tangential migration to the OB; however, upon arrival to the OB, the neuroblasts were distributed aberrantly within the radial dimension, and many immature neuroblasts failed to exit the rostral migratory stream. Conditional deletion of *Tshz1* in mice resulted in OB hypoplasia and severe olfactory deficits. We therefore investigated olfaction in human subjects from families with congenital aural atresia that were heterozygous for *TSHZ1* loss-of-function mutations. These individuals displayed hyposmia, which is characterized by impaired odor discrimination and reduced olfactory sensitivity. Microarray analysis, in situ hybridization, and ChIP revealed that TSHZ1 bound to and regulated expression of the gene encoding prokineticin receptor 2 (PROKR2), a G protein–coupled receptor essential for OB development. Mutations in *PROKR2* lead to Kallmann syndrome, characterized by anosmia and hypogonadotrophic hypogonadism. Our data indicate that TSHZ1 is a key regulator of mammalian OB development and function and controls the expression of molecules involved in human Kallmann syndrome.

Introduction

The olfactory bulb (OB) relays odor information from sensory neurons of the olfactory epithelium to higher brain centers. Interneurons located within the granule cell and glomerular layers modulate the OB's output through synaptic connections with mitral and tufted cell projection neurons. Remarkably, OB interneurons arise not only during embryonic development, but continue to be generated postnatally by neural stem cells located in regions derived from the dorsolateral ganglionic eminence (dLGE), i.e., the subventricular zone (SVZ) and subependymal zone adjacent to the lateral ventricles and within the rostral migratory stream (RMS). Neuroblasts reach the OB via tangential chain migration within the SVZ/RMS, a process that occurs throughout the entire postnatal life of rodents and during the first year of postnatal life in humans (1–7). Upon arrival in the OB, dLGE-derived interneuron progenitors migrate radially within the enlarging bulbs, mature, and integrate into the granule cell layer or the glomerular layer (8).

One molecule expressed in the developing OB and dLGE is teashirt zinc finger family member 1 (TSHZ1) (9). The founding member of the teashirt family, *tsh*, was first identified in *Drosophila* as a homeotic gene important for regulating head-trunk specification, with additional functions in patterning of the fly cuticle via modulation of the wingless (Wnt) signaling pathway (10, 11). Interestingly, *tsh* overexpression in *Drosophila* imaginal discs resulted in ectopic eye formation, a function previously attributed to the *Pax6/PAX6* homolog *eyeless*, which indicated that *tsh* lies near the top of the genetic hierarchy controlling organ development in the fly (12). 3 murine homologs of *tsh* were later identified (*Tshz1*, *Tshz2*, and *Tshz3*), encoding zinc finger proteins containing 3 atypical widely spaced zinc finger motifs, a homeodomain, and 2 classical zinc fingers (13). In the mouse, *Tshz1* was found to be essential for correct formation of the middle ear, the axial skeleton, and the soft palate (14), but to our knowledge, no functional analysis in the central nervous system has been published.

Here, we used classical and conditional mutagenesis in mice to investigate the roles of *Tshz1* in OB development and function. We found that OB neuroblast differentiation depended on *Tshz1*, with the majority of interneurons of the granule cell layer and a subpopulation of periglomerular neurons being absent in *Tshz1* mutant mice. Furthermore, in these animals, we noted that the radial migration of neuroblasts within the OB was severely impaired, a phenotype accompanied by severe OB hypoplasia. Interestingly, behavioral testing of mutant mice revealed marked olfactory deficits. Our findings with mice prompted us to study human individuals carrying heterozygous mutations in *TSHZ1*, which were recently described to cause congenital aural atresia (CAA), a congenital malformation of the external auditory canal (15). Intriguingly, we found significant reductions in olfactory sensitivity and discrimination in these patients, whereas

Authorship note: Daniela Ragancokova and Elena Rocca contributed equally to this work.

Conflict of interest: The authors have declared that no conflict of interest exists.

Citation for this article: *J Clin Invest.* 2014;124(3):1214–1227. doi:10.1172/JCI72466.

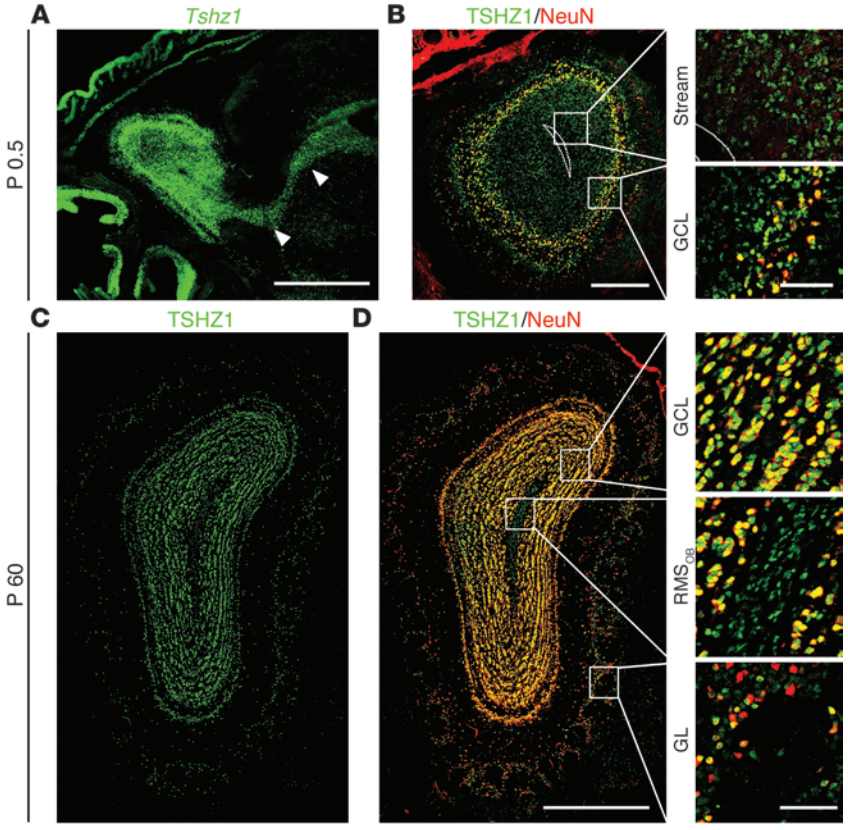

Figure 1
Tshz1 expression in developing and postnatal OB. (**A**) Sagittal sections of P0.5 forebrains showed a stream of cells migrating from the dLGE in a rostral direction toward the OB (arrowheads). *Tshz1*$^+$ cells (green, *Tshz1* mRNA) were located in this stream. (**B**) Coronal section of embryonic OB revealed cells expressing TSHZ1 protein (green) weakly in the stream (dotted outline), while in the granule cell layer (GCL), TSHZ1 was strongly expressed together with the neuronal differentiation marker NeuN (red). (**C** and **D**) In adult OB (P60), TSHZ1 (green) was prominently expressed together with NeuN (red) in neurons of the granule cell layer and with a subpopulation of neurons in the glomerular layer (GL). TSHZ1 was also weakly expressed within migrating cells of the RMS$_{OB}$ that were not NeuN$^+$. Scale bars: 1 mm (**A**); 500 μm (**C** and **D**); 200 μm (**B**); 50 μm (**B** and **D**, insets).

odor identification was relatively unchanged. Molecular analyses of OBs of *Tshz1* mutant mice showed reduced expression of the mRNA encoding for the G protein–coupled receptor prokineticin receptor 2 (PROKR2). Previous studies showed that signaling upon binding of the ligand prokineticin 2 (PK2) to PROKR2 plays central roles in neurogenesis and OB development, implicating this signaling system in neuroblast migration out of the RMS (16–18). Additionally, mutations in human *PROKR2* and *PK2* are among those that lead to Kallmann syndrome, which is characterized by anosmia, hypoplastic OBs, and hypogonadism (19, 20). Based on ChIP analysis of murine OB tissue, we suggest that the role of TSHZ1 in OB development and function may be mediated, at least in part, through its direct binding to regulatory elements within *Prokr2*, thereby promoting the radial migration of neuroblasts in the OB. Thus, TSHZ1 is a transcriptional regulator that impinges on genes involved in Kallmann syndrome and contributes to interindividual variation in olfaction in humans.

Results

Tshz1 expression in the olfactory system. We generated polyclonal antibodies against TSHZ1 for immunohistological and biochemical analyses. TSHZ1 expression was found in a stream of cells extending from the walls of the lateral ventricle to the OB as well as in cells scattered throughout the embryonic OB (Figure 1, A and B, and ref. 9). Stronger TSHZ1 expression was observed in the granule cell layer, where TSHZ1 was coexpressed with the neuronal differentiation marker NeuN (also known as RBFOX3; ref. 21). Weak expression of TSHZ1 was found postnatally in the RMS of the OB (RMS$_{OB}$), with stronger expression in the granule cell layer and a subpopulation of periglomerular neurons (Figure 1, C and D). Immunostaining with antibodies against NeuN revealed that the majority of TSHZ1$^+$ cells in the neuronal layers of the OB were differentiated neurons.

Tshz1 mutation affects the distribution and differentiation of granule cell neurons of the developing OB. We next used targeted mutations to analyze *Tshz1* function in murine OB (see Methods and Supplemental Figure 1, A–D; supplemental material available online with this article; doi:10.1172/JCI72466DS1). A cassette encoding GFP was introduced into the *Tshz1* locus to serve as a reporter of gene expression, with concomitant disruption of *Tshz1* protein-coding sequences. In order to circumvent the embryonic lethality of homozygous *Tshz1*-null mutants, we established mice with a *Tshz1*^{flox} allele and crossed these with animals harboring the *nestin-cre* transgene (22) to generate *nestin-cre;Tshz1*$^{GFP/flox}$ mice, with conditional mutation of *Tshz1* (referred to herein as coTshz1 mutant mice). The success of both gene targeting strategies was confirmed by analysis of GFP and TSHZ1 expression in OBs of control *Tshz1*$^{GFP/+}$ and *Tshz1*$^{GFP/flox}$ mice and loss of TSHZ1 expression at the protein and mRNA levels in *Tshz1*$^{GFP/Δ}$ and coTshz1 mutant mice (Supplemental Figure 1, E–H). Macroscopic examination of the brains of coTshz1 mutants at birth indicated no drastic change in OB size at this stage; similarly, upon histological examination, OBs of coTshz1 mutant mice appeared indistinguishable from those of controls (Figure 2, A and B). Immunostaining of OBs of control mice with antibodies directed against GFP revealed a ring of GFP$^+$ cells in the outer granule cell layer, whereas in coTshz1 mutants, GFP$^+$ cells were unevenly distributed as aggregates located mainly within the inner granule cell layer/SVZ (Figure 2C and Supplemental Figure 1, E and F). We examined whether neuronal differentiation was impaired in coTshz1 mutants at birth by

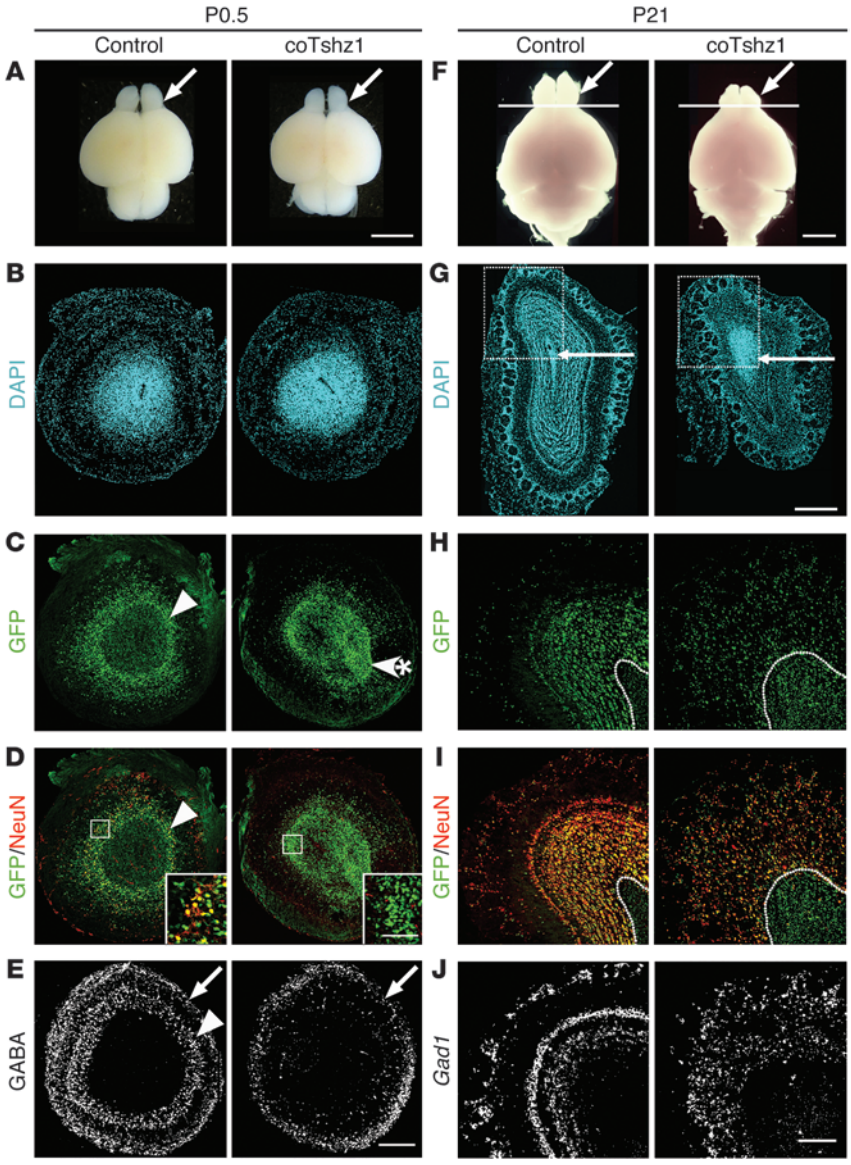

Figure 2
Tshz1 mutation affects the distribution and differentiation of granule cell neurons of developing and postnatal OB. Animals were analyzed at P0.5 (**A**–**E**) and P21 (**F**–**J**). OBs were examined either macroscopically (**A** and **F**; arrows denote OB) or after sectioning. Coronal sections show the whole OB (**B**–**E** and **G**) or part of the OB at higher magnification (**H**–**J**, boxed regions in **G**). Line in **F** denotes the OB/forebrain border. OBs were also examined by histology using DAPI (**B** and **G**); by immunohistology with antibodies directed against GFP (green, **C**, **D**, **H**, and **I**), NeuN (red, **D** and **I**), or GABA (white, **E**); or by in situ hybridization with a probe against *Gad1* (white, **J**). Note that **C** and **D** as well as **H** and **I** show images from the same sections. Arrowheads in **C**–**E** denote the outer granule cell layer; arrows in **E** denote the glomerular layer; arrowhead with asterisk in **C** denotes the GFP^+ aggregates observed in coTshz1 mutants; arrows in **G** denote the RMS_{OB}; dotted lines in **H** and **I** outline the RMS_{OB} border. Scale bars: 3 mm (**A**); 500 μm (**G**); 200 μm (**B**–**E** and **H**–**J**); 50 μm (**D**, insets).

immunostaining for NeuN, GABA, and tyrosine hydroxylase (TH). Loss of these markers was observed in the outer granule cell layer of coTshz1 as well as homozygous null mutant mice, while GABA and TH expression in the glomerular layer was unchanged (Figure 2, D and E, and Supplemental Figure 1, I and J). We also analyzed the organization of the mitral cell layer by immunostaining for TSHZ2 and detected no changes at P0.5 in homozygous null or coTshz1 mutants (Supplemental Figure 1, E and F). Whereas homozygous $Tshz1^{GFP/\Delta}$ and $Tshz1^{GFP/GFP}$ mutants died within 24 hours of birth, displaying aerophagia, coTshz1 mutant mice suckled milk, with 30% surviving to adulthood. However, growth and body weight gain in coTshz1 mutants were severely impaired (Supplemental Figure 2 and Supplemental Methods).

Tshz1 mutation affects maturation of granule cell neurons of the postnatal OB. We next investigated the role of *Tshz1* in postnatal OB maturation. Macroscopic examination revealed that the OBs of postnatal coTshz1 mutants were substantially smaller than those of controls, while overall brain size was much less affected (Figure 2F), suggestive of aberrant generation and/or migration of neurons that move to the OB. Whereas DAPI staining demonstrated the classical layered architecture of the OB in control mice, coTshz1 mutants displayed a severely disrupted OB: the granule cell and external plexiform layers could not be discerned, the glomerular layer was multilayered, and the RMS_{OB} was markedly thickened (Figure 2G). Immunostaining with antibodies against GFP and NeuN revealed weak expression of the GFP reporter within the RMS_{OB} in control $Tshz1^{GFP/flox}$ mice, with stronger staining throughout the differentiated $NeuN^+$ cells of the granule cell and external plexiform layers as well as in a subpopulation of periglomerular neurons (Figure 2, H and I). In coTshz1 mutants, the GFP^+ RMS_{OB} was much more prominent, both in size and with respect to the strength of GFP staining, while the number of $NeuN^+GFP^+$ differentiated interneurons surrounding the RMS and extending up to the glomerular layer was substantially reduced (Figure 2, H and I). In situ hybridization with probes against *Gad1* revealed a substantial reduction in the number of GABAergic cells in

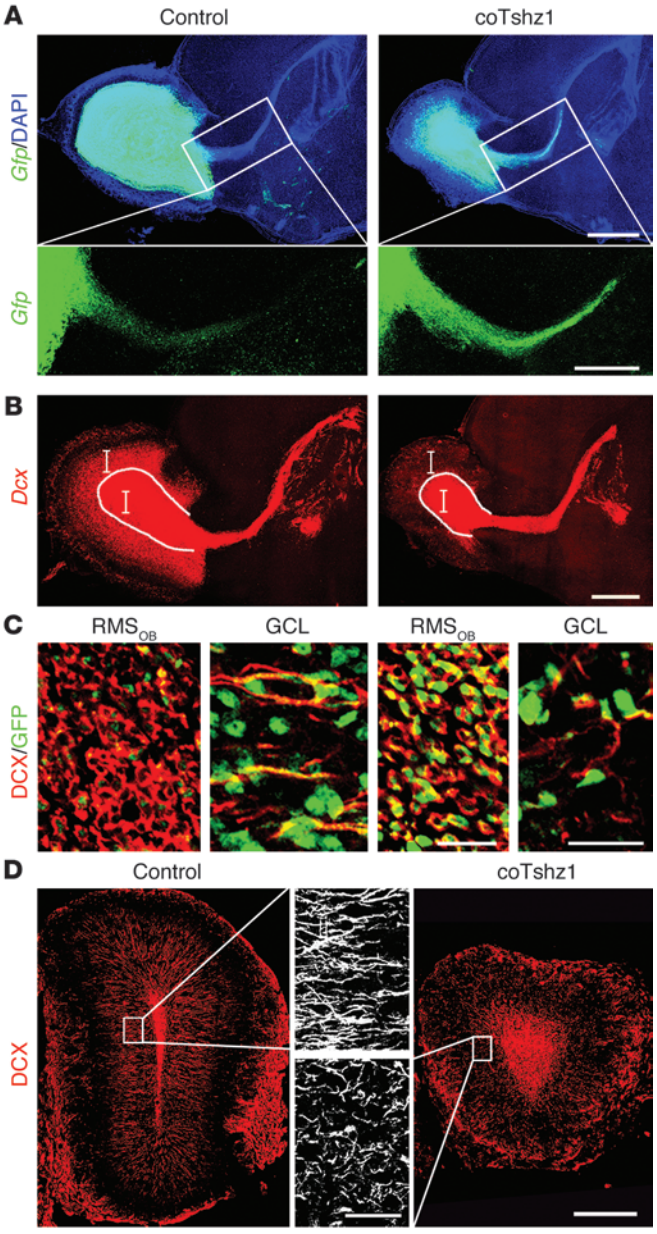

Figure 3
Impaired radial migration of neuroblasts from the RMS_{OB} in the absence of *Tshz1*. Shown are sagittal sections of the OB and rostral forebrain (**A** and **B**) or coronal sections of the adult OB (**C** and **D**). Tissue was analyzed by in situ hybridization with probes against *Gfp* (green, **A**) or *Dcx* (red, **B**) or with antibodies directed against GFP (green, **C**) or DCX (red, **C** and **D**). Sagittal sections were also counterstained with DAPI (blue, **A**). White dotted line in **B** denotes the border between the RMS_{OB} and cells that have switched to radial migration; vertical brackets in **B** denote sectional planes corresponding to images in **C**. (**C**) Note the presence of radially oriented DCX^+ processes of migrating neuroblasts that also stained for GFP in the granule cell layer of control mice. (**D**) Neuroblasts immunostained for DCX were present in the RMS_{OB} and also dispersed throughout the granule cell layer in control mice, but had accumulated in the RMS_{OB} in coTshz1 mutants. Insets: DCX^+ processes (white) were radially oriented in control mice, whereas no clear orientation was apparent in mutant mice. Scale bars: 1 mm (**A** and **B**); 500 μm (**D** and **A**, insets); 50 μm (**D**, insets); 25 μm (**C**).

coTshz1 mutant OBs (Figure 2J). Thus, *Tshz1* plays a dual role, both in the distribution and in the differentiation of granule cell neurons of the developing and postnatal OB.

Tshz1 mutation affects radial migration of neuroblasts from the RMS_{OB}. We next examined the morphology of the RMS along its route from the lateral ventricles toward the OB by in situ hybridization using RNA probes against *Gfp* and doublecortin (*Dcx*). No clear alterations in the size of the RMS prior to entering the OB were seen (Figure 3, A and B, and Supplemental Figure 3); however, upregulation of *Gfp* mRNA was observed within the entire RMS of coTshz1 mutants (Figure 3A), implying negative autoregulation of *Tshz1* expression. In situ hybridization with a *Dcx* probe on sagittal sections of control mice revealed a core region of strong *Dcx* expression corresponding to the RMS_{OB} that was surrounded by a more dispersed zone of *Dcx* $mRNA^+$ neuroblasts moving away into the granule cell layer (Figure 3B). In coTshz1 mutants, dispersion of cells away from the RMS_{OB} was significantly reduced, with only the RMS_{OB} being clearly apparent. Immunostaining with antibodies directed against DCX and GFP on coronal sections of control mice demonstrated the presence of GFP^+DCX^+ migrating neuroblasts in the RMS_{OB}, as well as radially oriented DCX^+ processes extending from the RMS_{OB} through the granule cell layer (Figure 3, C and D, and ref. 23). Such DCX^+ processes coexpressed GFP and were interdigitated between the strongly GFP^+ neurons of the granule cell layer in control mice (i.e., migrating DCX^+ neuroblasts in the granule cell layer belong to the *Tshz1* lineage; Figure 3C). The markedly thickened RMS_{OB} of coTshz1 mutants was characterized by accumulation of DCX^+ neuroblasts that strongly expressed GFP, while radially oriented DCX^+ processes outside the RMS_{OB} could not be found (Figure 3, C and D).

Alterations in the number and distribution of OB interneurons and in the size of the RMS_{OB} could reflect changes in proliferation of neural stem cells or their progeny, or aberrant migration/differentiation of neuroblasts within the OB. We therefore injected BrdU into mice and analyzed the number of $BrdU^+$ cells in the OB 2 hours later or after a chase of 1 or 2 weeks (Figure 4). We chose this time window based on previous studies in which it was shown that a newly born neuroblast in the SVZ takes approximately 1 week to migrate tangentially into the RMS_{OB} and begin radial migration, and a further week to become a differentiated neuron of the granule cell layer (24). At 2 hours after BrdU injection, we observed ~0.5% proliferating cells in the RMS_{OB} in controls, whereas coTshz1 mutants showed an approximately 2.5-fold increase in proliferation (Figure 4B). At 1 week after injection of control animals, many $BrdU^+$ cells were found in the RMS_{OB}, similar to the density in coTshz1 mutants (control, 54 ± 4 cells/100-μm quadrant; coTshz1, 38 ± 8 cells/100-μm quadrant; P = NS). The proportion of $BrdU^+$ cells within the RMS_{OB} was unchanged at this time point (Figure 4C), which suggests that tangential migration was not severely affected in coTshz1 mutants. After 2 weeks of chase, most $BrdU^+$ cells in control animals had exited the RMS_{OB} and differentiated into granule cell neurons, whereas in coTshz1 mutants, considerably more $BrdU^+$ cells remained stuck in the RMS_{OB} (Figure 4D). We next determined the displacement of $BrdU^+$ cells from the anatomical midline of the RMS_{OB} at 2 weeks of chase. A significantly higher proportion of $BrdU^+$ cells were present within 25 μm of the RMS_{OB} midline in coTshz1 mutants (Figure 4, E and F), indicative of impaired radial migration. We also determined the fate of

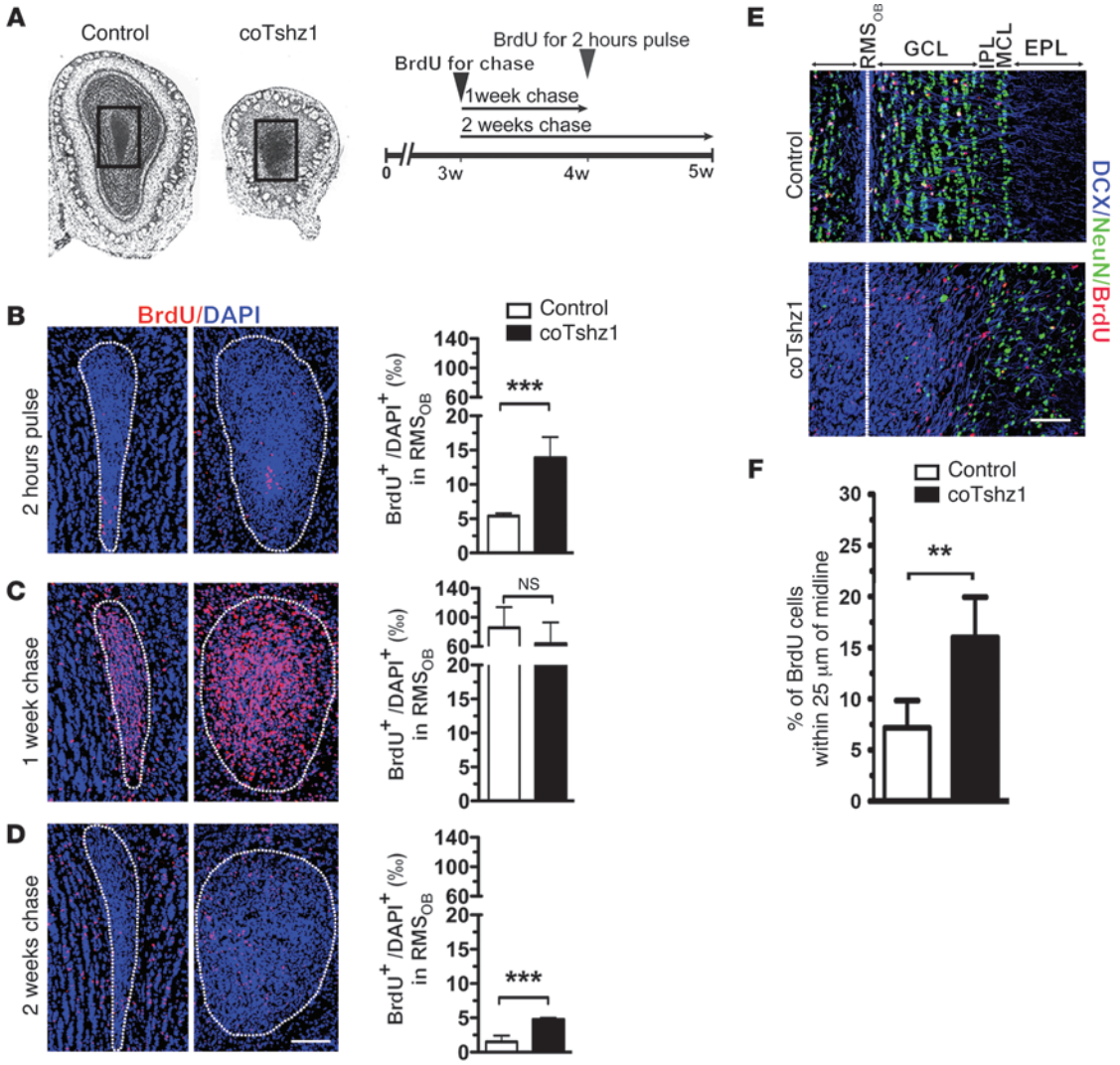

Figure 4

Tangential and radial migration in coTshz1 mutants. (**A**–**D**) After injection with a pulse of BrdU and chasing for different lengths of time (**A**), $BrdU^+$ cells (red, **B**–**D**) within the RMS_{OB} (dotted white lines) were examined by immunohistology (blue, DAPI counterstain). Boxed regions in **A** denote areas analyzed in **B**–**D**. Per mil of $BrdU^+$ cells in the RMS_{OB} were also quantitated relative to total $DAPI^+$ cells. (**E**) Coronal sections of 5-week-old OBs were analyzed after a 2-week chase and immunostained for BrdU (red), DCX (blue), and NeuN (green). Note the presence of many $BrdU^+$ cells within the enlarged RMS_{OB} of coTshz1 mutants containing DCX^+ neuroblasts. The external plexiform layer (EPL), mitral cell layer (MCL), internal plexiform layer (IPL), granule cell layer, and RMS_{OB} are indicated, as well as the anatomical midline of the RMS_{OB} (dotted white line). (**F**) Percentage of $BrdU^+$ cells located within 25 μm of the midline of the RMS_{OB} in control and coTshz1 mice after a 2-week chase. Scale bars: 100 μm (**B**–**E**). $^{**}P < 0.01$; $^{***}P < 0.001$.

postnatally generated cells in coTshz1 mutants by immunostaining OBs for NeuN and BrdU at the 2-week chase time point and noted a significant increase in the proportion of cells in coTshz1 mutants that had incorporated BrdU, but failed to differentiate into $NeuN^+$ granule cell neurons (Figure 4E and Supplemental Figure 4). To determine whether the increased number of undifferentiated neuroblasts in coTshz1 mutants was accompanied by alterations in cell death, we performed TUNEL staining and found a significantly higher number of apoptotic cells in these animals (Supplemental Figure 5). We conclude that tangential migration of neuroblasts toward the OB proceeds normally in the absence of *Tshz1*, whereas radial migration of neuroblasts out of the RMS_{OB} into the granule cell layer of the OB is markedly reduced. Furthermore, the differentiation of postnatally generated neuroblasts within the OB of coTshz1 mutants was severely impaired and accompanied by increased programmed cell death.

Tshz1 is required for generation of calbindin-positive periglomerular interneurons. Periglomerular neurons of the glomerular layer of the OB also emerge from the embryonic and postnatal RMS_{OB} (25). They receive synaptic input from olfactory receptor cell axon terminals and form dendrodendritic synapses onto mitral/tufted cell dendrites. Whereas the number of dopaminergic TH^+ and calretinin-positive (CR^+) periglomerular neurons was relatively unchanged (Figure 5, A–D), a large reduction in the

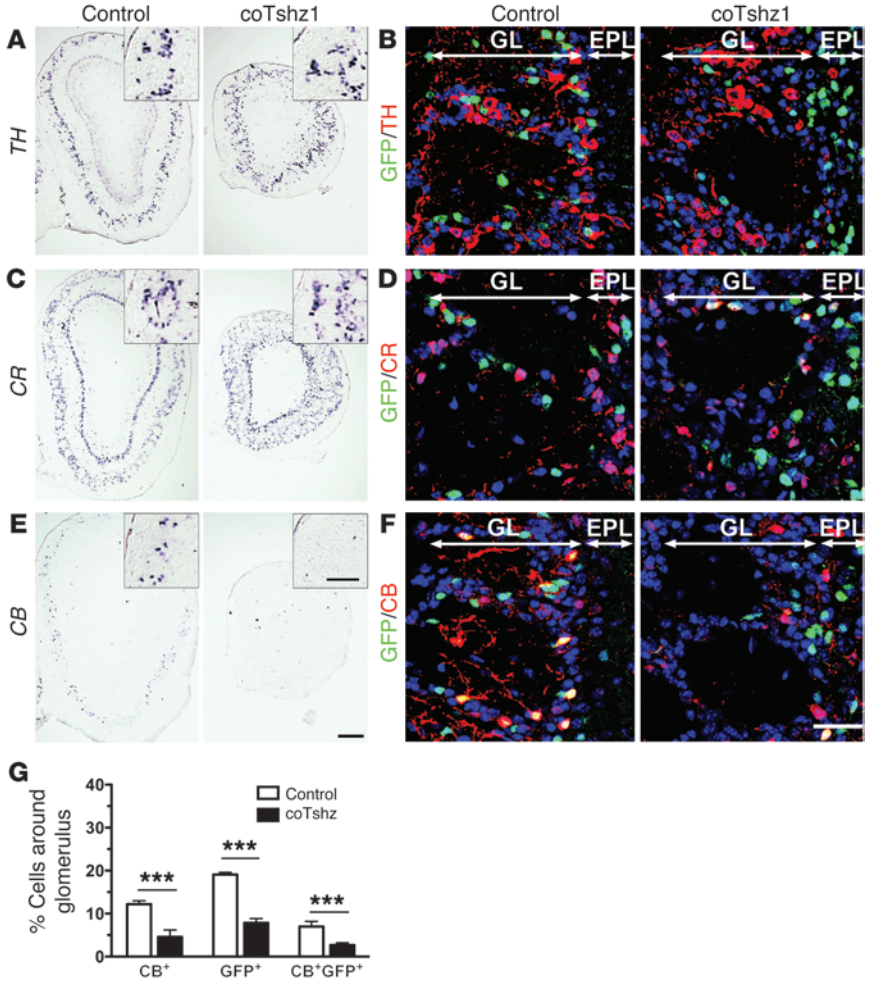

Figure 5
Analysis of periglomerular neurons in postnatal control and coTshz1 mutant mice by in situ hybridization or immunohistology. Coronal sections were stained using in situ probes against *TH*, *CR*, or *CB* (**A**, **C**, and **E**; insets highlight glomerular layer) or immunostained for these markers (red) in the glomerular layer, together with GFP (green) and DAPI counterstaining (blue) (**B**, **D**, and **F**). No clear alterations in the expression of TH (**A** and **B**) or CR (**C** and **D**) were seen in the glomerular layer of coTshz1 mutant animals. In contrast, the number of CB^+ periglomerular neurons was reduced in coTshz1 mutant mice (**E**–**G**). Glomerular and external plexiform layers are indicated. Scale bars: 300 μm (**A**, **C**, and **E**); 100 μm (**A**, **C**, and **E**, insets); 50 μm (**B**, **D**, and **F**). ***$P < 0.001$.

number of calbindin-positive (CB^+) periglomerular neurons was observed using in situ hybridization or immunostaining (Figure 5, E–G). Furthermore, in coTshz1 mutants, fewer GFP^+ cells surrounded the outer parts of the glomeruli (Figure 5G). We also analyzed expression of PAX6, a transcription factor that regulates the generation of a subpopulation of periglomerular neurons (26, 27). In control mice, the expression patterns of PAX6 and *Tshz1* (using GFP immunostaining) revealed nonoverlapping populations of periglomerular neurons (Supplemental Figure 6A). Interestingly, in coTshz1 mice, we observed an increase in the number of $PAX6^+$ cells surrounding glomeruli, which was accompanied by the presence of ectopic GFP^+PAX6^+ cells (Supplemental Figure 6), suggestive of functional antagonism between *Pax6* and *Tshz1* in periglomerular neurons. Thus, we conclude that beyond its role in the development of granule cell neurons, *Tshz1* also regulates the migration and/or differentiation of a subpopulation of periglomerular neurons in the postnatal OB, some of which express CB.

Tshz1 mutations lead to poor sense of smell in mice. In order to determine whether the alterations observed in the granule cell and periglomerular layers of the OB affect olfactory function in coTshz1 mutant mice, we carried out behavioral tests. In contrast to control animals, 11 of 13 coTshz1 animals could not find a buried food pellet, whereas food previously soaked in 64 μM vanillin was detected, with latencies approaching those seen in controls (Figure 6A). We next carried out an odor preference test, in which control mice showed a tendency to avoid 2-methyl butyric acid (an unpleasant odor) and a marked preference for peanut butter (a pleasant odor) compared with the time spent investigating a filter paper dosed with water (Figure 6B). coTshz1 mutants were more interested in water than control animals, and no significant differences in preference for 2-methyl butyric acid or peanut butter were observed. Next, in response to 3 consecutive presentations of the same odor, habituation was observed in coTshz1 mutants, but the responses to changes of odor (i.e., dishabituation) were markedly reduced (Figure 6C). In addition, coTshz1 mutants failed to respond to the odor 2,3,5-trimethyl-3-thiazoline (TMT), even when presented at concentrations 100-fold higher than those required to elicit a response in control animals (Supplemental Figure 7A). We therefore conclude that the olfactory function of coTshz1 mutant mice is severely compromised.

TSHZ1 mutations in humans influence sense of smell. Encouraged by these results in mice, we next sought to determine whether *TSHZ1* influences olfactory function in humans. Heterozygous mutations in *TSHZ1* were recently characterized in families with CAA, including those carrying deletions in 18q22.3 as well as point mutations in *TSHZ1* coding sequences (15). Olfactory function was tested in 5 individuals heterozygous for *TSHZ1*

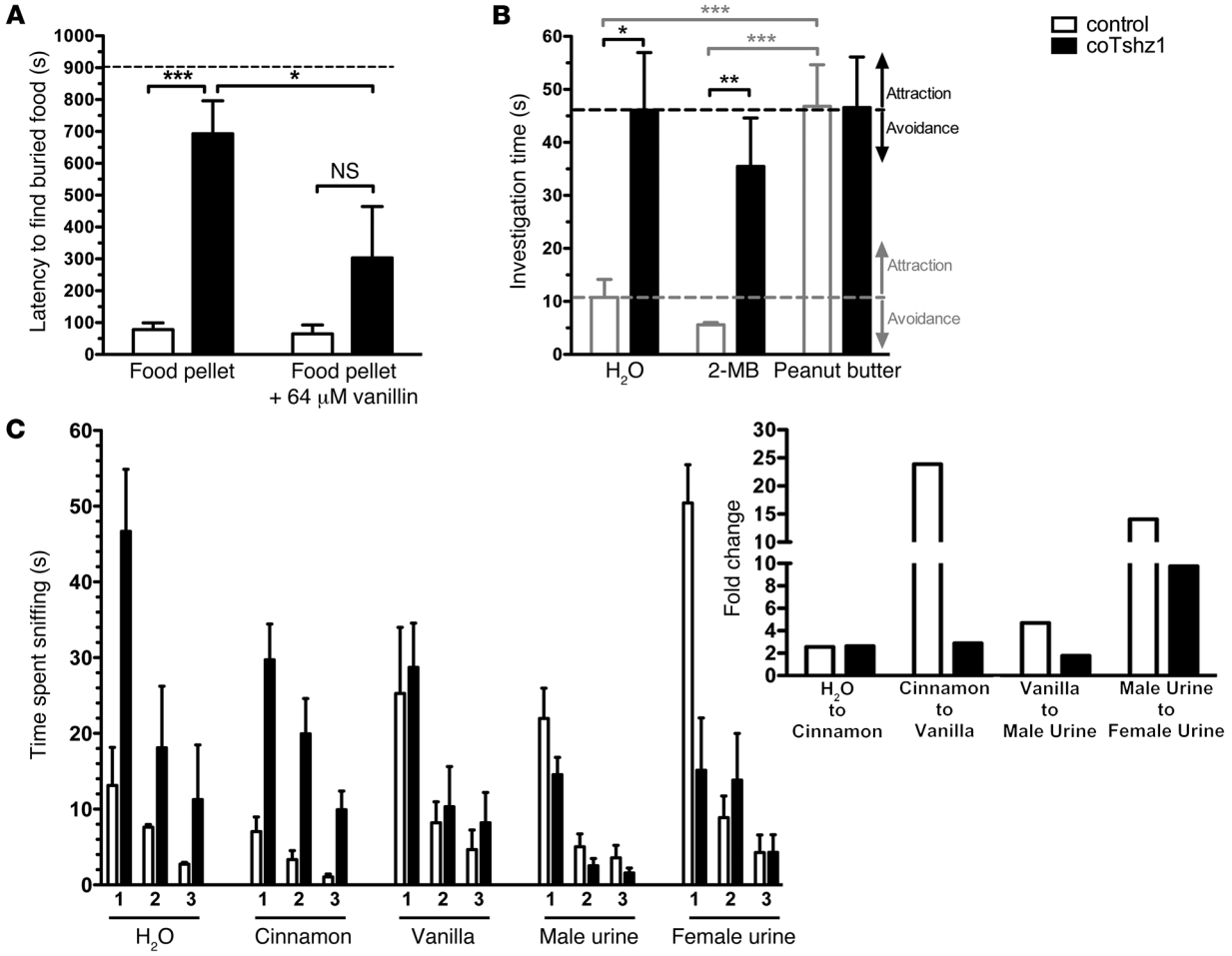

Figure 6

Tshz1 mutations in mice result in severe olfactory deficits. (**A**) Buried food test. The latency of coTshz1 mutant mice to find hidden food pellets substantially increased, although these mice were capable of food detection after soaking pellets in vanillin. Dashed line denotes the maximal 15-minute test period (900s). (**B**) Preference test. Time spent sniffing at filter papers containing 1 of 3 odors (water, 2-methyl butyric acid [2-MB], and peanut butter, presented in random order) was determined. Whereas control mice tended to avoid 2-MB and were strongly attracted to peanut butter, no clear responses to aversive or attractive odors were seen in coTshz1 mutants. Gray and black dashed lines denote the investigation time of neutral odor (H_2O) of control and coTshz1 mutant mice, respectively. (**C**) Habituation/dishabituation test. Animals were presented 3 times with different odors on cotton swabs in the order shown, and total time spent sniffing was determined. Inset shows fold change in investigation time in response to the presentation of a new smell (i.e., third test of previous odor compared with first test of next odor). $^*P < 0.05$; $^{**}P < 0.01$; $^{***}P < 0.001$.

mutations (Figure 7A) together with age- and sex-matched controls, using filter pens containing different odors (28). The mutant *TSHZ1* alleles harbor point mutations that result in premature stop codons and encode severely truncated mutant proteins with predicted loss of function (Table 1 and ref. 15). Clinical and genetic details of the individuals tested are shown in Tables 1 and 2. Intriguingly, substantial decreases in odor sensitivity and impaired odor discrimination were found in all 5 patients, while odor identification did not differ between the control and the mutant groups (Figure 7, B and C). Thus, haploinsufficiency of *TSHZ1* perturbed olfactory function in humans, which resulted in hyposmia. We noted no significant changes in olfactory function in mice heterozygous for a loss-of-function *Tshz1* mutation ($Tshz1^{GFP/flox}$) (Supplemental Figure 7B), which indicates that humans are more sensitive to alterations in *TSHZ1* gene dosage than rodents with respect to olfaction.

Expression of Prokr2, which encodes a molecule that regulates OB interneuron migration, depends on Tshz1. In order to better understand the molecular changes occurring downstream of *Tshz1* function in the developing and postnatal OB, we used microarray hybridization to profile gene expression in control and *Tshz1* mutant mice at the embryonic and postnatal stages (E18.5 and P30, respectively; see Methods). A panel of mRNAs whose expression was altered (Figure 8A) was then analyzed by in situ hybridization on sections of OBs of postnatal coTshz1 mutants (Figure 8, C–F, H–K, and M–P). In addition, probes against *Tshz1* or *Gfp* were used, as well as *Reelin*, a marker of mitral cells, whose expression was retained in coTshz1 mutants but revealed a somewhat disorganized mitral cell layer (Figure 8, B, G, and L). Several markers of the granule cell layer — including syntabulin (*Sybu*), sorting nexin 7 (*Snx7*), *Krox20/Egr2*, and the immediate early gene *Arc* — were downregulated in the OB of coTshz1 mutants, in accordance with

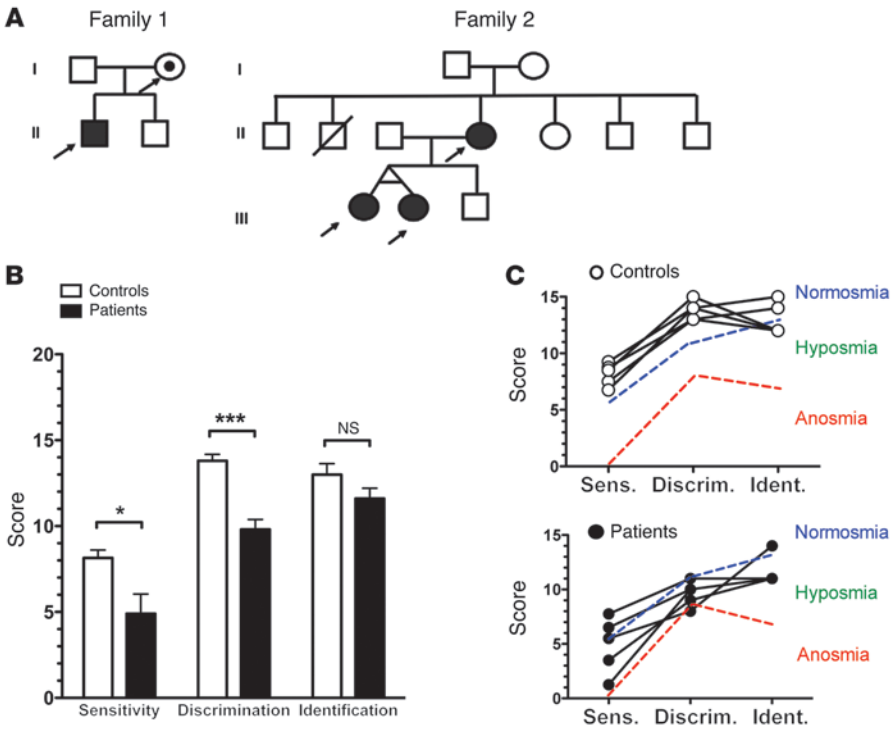

Figure 7

TSHZ1 mutations lead to hyposmia in humans. (**A**) Pedigrees of the 2 families with CAA and *TSHZ1* mutations. Families 1 and 2 correspond to families 3 and 4, respectively, as previously described by Feenstra et al. (15). Arrows denote heterozygous *TSHZ1* mutations; black symbols denote individuals presenting with CAA. The mother in family 1 carried the mutation, but did not have CAA (Table 1). (**B** and **C**) Olfactory performance was assessed using Sniffin' Sticks in 3 tests in patients heterozygous for *TSHZ1* and in age- and sex-matched controls. Data are presented as (**B**) mean ± SEM and as (**C**) data points for each individual, with lines connecting each of the 3 tests. Olfactory scores on or above the dotted blue line are indicative of normosmic individuals, those between the dotted blue and red lines indicate hyposmic individuals, and those below the dotted red line indicate anosmic individuals. Note the reduced olfactory scores for sensitivity and discrimination in the patients (see also Tables 1 and 2). $^{*}P < 0.05$; $^{***}P < 0.001$.

a major deficit in granule cell differentiation. Intriguingly, among the most significantly changed transcripts in the microarray data at E18.5 and postnatally was *Prokr2*. Expression of *PK2* was also downregulated in the RMS_{OB} of postnatal animals. We therefore analyzed *Prokr2* expression in the developing OB of control and *Tshz1* mutant mice at E18.5 using in situ hybridization. Whereas *Tshz1* mRNA marked both the outer granule cell layer and more immature cells within the inner layers of the OB, *Prokr2* expression was restricted to the inner layers of the OB in control mice at E18.5 (Figure 9, A and B). In *Tshz1* mutants, *Prokr2* expression was strongly downregulated (Figure 9B).

The enlarged RMS_{OB} and smaller OBs observed in postnatal coTshz1 mutants strongly resembled the phenotypes observed in mice with mutations in *Prokr2* or *PK2*, and humans with Kallmann Syndrome carrying mutations in *PROKR2* or *PK2* have hypoplastic OBs (16–20). In postnatal control mice, *Prokr2* was expressed in cells both within the RMS_{OB} and in a subpopulation surrounding the RMS_{OB} that was scattered through the granule cell layer (Figure 9C), presumably corresponding to radially migrating neuroblasts. In coTshz1 mutants, *Prokr2* expression within the enlarged RMS_{OB} was slightly downregulated; importantly, no cells were seen outside the RMS that still expressed *Prokr2*. Expression of *PK2* was seen in a subpopulation of granule cells within the control OB, but was essentially extinguished in coTshz1 mutant mice (Figure 9D), similar to the loss of expression observed for several other markers of granule cells (Figure 8). *Prokr2* expression in cells of the SVZ as well as in neuroblasts migrating tangentially within the RMS was not affected by *Tshz1* mutation (Supplemental Figure 8, A–C), which suggests that the function of *Tshz1* in regulating *Prokr2* expression is confined to the RMS_{OB}, similar to what was seen at embryonic stages. We therefore conclude that in the absence of *Tshz1*, accumulation of neuroblasts within the RMS_{OB} is accompanied by a major loss of PROKR2-dependent signals.

ChIP reveals association of TSHZ1 with the Prokr2 gene in vivo. We sought to determine whether TSHZ1 physically associates with the *Prokr2* locus (Figure 9E) by performing ChIP experiments on murine OB tissue using our anti-TSHZ1 polyclonal antiserum. Western blot analysis of OB lysates demonstrated that the TSHZ1 antiserum used in ChIP recognized a protein species with the size expected for TSHZ1 (Supplemental Figure 8D). We designed primer pairs located within different regions of *Prokr2*, either covering the promoter region (1.6 kb) or situated within the first intron flanking a region containing sequences conserved between the murine promoters of *Sybu*, *Prokr2*, and *Tshz1*, as well as an element highly conserved across different mammals in the promoter region of *Tshz2*. No consistent ChIP enrichment was found within the promoter of *Prokr2* (Figure 9F). However, we observed enrichment for the region located toward the middle of intron 1 of *Prokr2* with anti-TSHZ1 antiserum, as determined by conventional PCR (Figure 9F). Quantitative PCR was then performed after ChIP of OB tissue across 5 biological replicates (4 animals each; see Methods). Significant enrichment for the region flanked by the primers within intron 1 of *Prokr2* was seen (2-fold enrichment versus promoter; $P = 0.018$; Figure 9G). Thus, we conclude that TSHZ1 physically interacts with chromatin in the first intron of the *Prokr2* locus.

Discussion

Characterization of loss-of-function mutations in *TSHZ1* in patients with CAA and 18q deletion syndrome previously highlighted the important role of this gene in human craniofacial development (15). Here, we identified hyposmia as another diagnostic criterion of CAA patients with *TSHZ1* mutations. Using targeted mutagenesis in mice, we were able to assign crucial key functions to *Tshz1* in the development and function of the OB, a structure with essential functions in processing incoming olfactory information

Table 1
TSHZ1 mutation–carrying individuals assessed in this study

Subject	Age (yr)	Sex	Relationship	Mutation	CAA type	Cognitive development	Olfactory scores		
							Sensitivity	Discrimination	Identification
Family 1									
1.I:2	43.1	Female	Mother of 1.II:1	c.723G>A, p.W241X	Normal	Normal	7.75	11	11
1.II:1	12.5	Male	Son of 1.I:2	c.723G>A, p.W241X	IIA, bilateral	Normal	1.25	10	11
Family 2									
2.II:4	44.7	Female	Mother of 2.III:1 and 2.III:2	c.946_947delinsA, p.P316TfsX16	IIA, bilateral	Normal	5.5	8	14
2.III:1	13.9	Female	Daughter of 2.II:4[A]	c.946_947delinsA, p.P316TfsX16	IIA, bilateral	Normal	6.5	11	11
2.III:2	13.9	Female	Daughter of 2.II:4[A]	c.946_947delinsA, p.P316TfsX16	IIA, bilateral	Normal	3.5	9	11

Families 1 and 2 correspond to families 3 and 4, respectively, as previously described by Feenstra et al. (15). Both the c.723G>A and c.946_947delinsA mutations lead to major truncations in the mutant TSHZ1 proteins (after 241 and 316 amino acids, respectively; wild-type TSHZ1 contains 1,032 amino acids), with predicted loss of function due to the loss of the majority of the protein sequence. [A]Twin.

from the olfactory epithelium and relaying this information to the olfactory cortex. We found that *Tshz1* was important for migration of neuroblasts of the granule cell lineage of the OB as well as for differentiation of granule cells and a subclass of periglomerular interneurons. These functions were in turn required for a normal sense of smell in rodents and humans.

Neurogenesis in the mouse occurs mainly during embryonic to early postnatal stages. However, in the adult rodent brain, there are 2 areas in which new neuroblasts are continually generated: the SVZ and the hippocampal subgranular zone, which migrate to the RMS_{OB} and integrate into the dentate gyrus of the hippocampus, respectively (29, 30). In humans, while hippocampal neurogenesis continues into adulthood (31), generation of neurons in the SVZ that migrate to the OB appears to cease within the first year of postnatal life (7). Using mice, we characterized the expression of *Tshz1* in the postnatal RMS and OB and used conditional mutagenesis to elucidate its function. *Tshz1* expression was weak within the RMS, becoming stronger along its route toward the RMS_{OB}, and could be identified in cells expressing doublecortin, a marker for migrating neuroblasts (23). The strongest site of *Tshz1* expression was that consisting of $NeuN^+$ granule cells and a subpopulation of $NeuN^+$ periglomerular neurons (32). In the absence of *Tshz1*, the tangential migration of DCX^+ neuroblasts along the RMS was unperturbed, whereas upon arrival in the OB, RMS_{OB} neuroblasts failed to orient their cellular processes toward the periphery of the OB, and did not migrate efficiently in the radial dimension. We found that this related to defects in PROKR2 signaling (see below). In addition, there was a profound failure of differentiation of granule cell neuroblasts in the OB. OB neurogenesis relies on coordination of multiple processes, including cell cycle control in the SVZ; tangential and radial migration of neuroblasts within the RMS and the RMS_{OB}, respectively; and differentiation and formation of synaptic connections in the OB. Both radial migration and neuronal differentiation were affected in the absence of *Tshz1*. This could reflect independent functions of *Tshz1* in these 2 processes or, alternatively, a primary effect of *Tshz1* on radial migration, leading secondarily to defects in differentiation. Interestingly, work on the factor p27Kip1 showed how it independently regulates neuronal differentiation and migration in newborn cortical neurons (33), and studies of basic helix-loop-helix factors showed that they have dual independent functions in migration and neurogenesis (34). shRNA-mediated knockdown of *Dcx* led to accumulation of cells within the RMS_{OB}, but did not affect the capacity of neuroblasts to differentiate into neurons, although changes in dendritic arbors were observed (35). Thus, the lack of granule cell differentiation in *Tshz1* mutants and the migratory deficit that leads to increased numbers of neuroblasts in the RMS_{OB} likely reflect independent functions for the factor in neurogenesis and migration.

It has previously been shown that OB volume positively correlates with olfactory function in children and during aging and is reduced in neuropsychiatric conditions, accompanied by losses in olfactory sensitivity (36, 37). We observed reduced olfactory sensitivity as well as impaired olfactory discrimination in human patients carrying heterozygous mutations in *TSHZ1*. Similarly, coTshz1 mutant mice showed significant olfactory impairments as well as displaying smaller OBs, likely as a result of reduced numbers of granule cells and consequent loss of substantial amounts of neuropil. Clinical examinations to determine OB volume,

Table 2
TSHZ1 control individuals assessed in this study

Subject	Age (yr)	Sex	CAA type	Cognitive development	Olfactory scores		
					Sensitivity	Discrimination	Identification
Control 1	43.0	Female	Normal	Normal	9.25	14	15
Control 2	13.4	Male	Normal	Normal	6.75	14	12
Control 3	43.5	Female	Normal	Normal	8.75	13	14
Control 4	13.5	Female	Normal	Normal	8.5	15	12
Control 5	13.6	Female	Normal	Normal	7.5	13	12

Control subjects were not related to each other and did not have *TSHZ1* mutations.

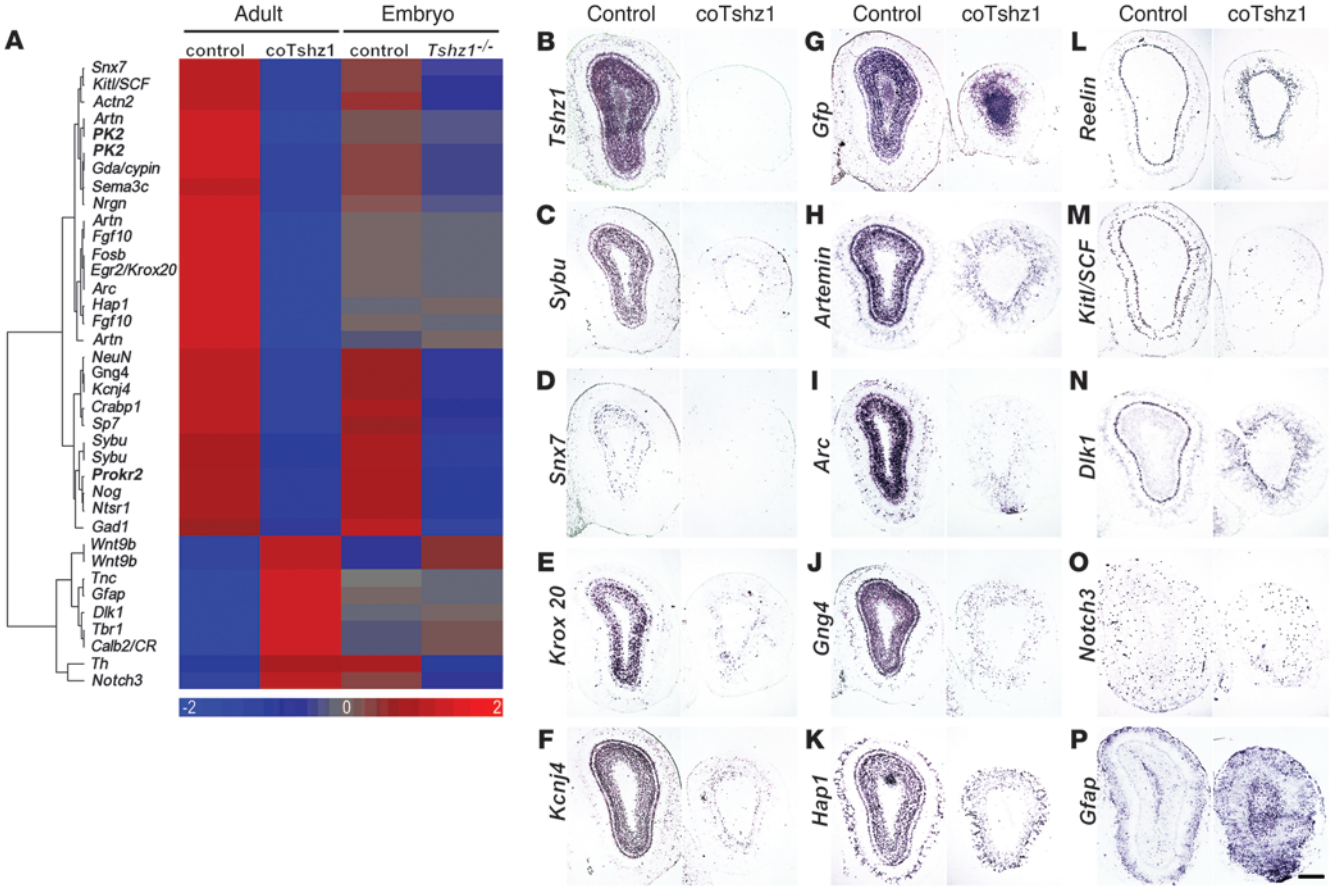

Figure 8

Microarray and mRNA expression analyses of OBs of embryonic and postnatal *Tshz1* mutant mice. (**A**) Cluster analysis of expression of selected genes (red, high expression; blue, low expression; $\log_2$ scale). (**B**–**P**) Coronal sections were analyzed by in situ hybridization using probes against *Tshz1* (**B**), *Gfp* (**G**), and *Reelin* (**L**) as well as those against a subset of differentially expressed mRNAs from the microarray screen, as indicated. Expression of these transcripts in coTshz1 mutants was (i) reduced in the granule cell layer and granule cells of the mitral cell layer (*Sybu*, **C**; *Snx7*, **D**; *Krox20*, **E**; *Kcnj4*, **F**; *Artemin*, **H**; *Arc*, **I**; *Gng4*, **J**; *Hap1*, **K**); (ii) reduced in the mitral cells and superficial tufted cells (*Kitl*/*SCF*, **M**); (iii) maintained in mitral cells (*Dlk1*, **N**) or in scattered cells of the OB (*Notch3*, **O**); or (iv) broadly increased throughout the OB (*Gfap*, **P**). Note that expression of the mitral cell layer marker *Reelin* (**L**) was retained in coTshz1 mutants, although some disorganization of the mitral cell layer was apparent. Scale bar: 300 μm.

including magnetic resonance imaging, could therefore be of diagnostic relevance in patients with bilateral CAA type 2a who also present with olfactory deficits. Based on our findings in mice, we suggest that the marked deficits in olfactory function resulting from mutation in *TSHZ1* in humans could be attributable to defects in the granule cell lineage, such as reduced numbers or impaired maturation of these neurons. The importance of granule cells in OB function has been previously shown in studies in mice that demonstrated olfactory impairments when the activity of granule cells had been silenced (38) or in mutant strains with reduced numbers of granule cells (39).

In contrast to the CAA and olfactory deficits seen in human $TSHZ1^{+/-}$ patients, heterozygous $Tshz1^{+/-}$ mice do not display middle-ear defects (14) or altered sense of smell (present study). We interpret this as showing that humans are more sensitive to alterations in *TSHZ1* gene dosage than rodents. Such differences between humans and mouse models have been previously noted; for example, heterozygous mutations in *NKX2.1* (encoding a transcription factor) lead to clear clinical phenotypes (40), whereas heterozygous $Nkx2.1^{+/-}$ mice develop normally, and phenotypes that parallel those seen in humans are observed only in homozygote animals (41).

We showed here that one major function of *Tshz1* in the OB of mice is to maintain the expression of *Prokr2*. Prokineticin signaling is involved in several biological processes, including nociception, circadian rhythm, and neurogenesis (17, 42, 43). PK2 and its receptor, PROKR2, are essential factors for normal OB development (16, 17). Both *PK2* and *Prokr2* mutant mice displayed an accumulation of immature neuroblasts in the RMS_{OB}, implicating PROKR2/PK2 signaling in the final steps of immature neuron migration in the OB, such as the dissociation of tangentially migrating neuroblast chains in the RMS_{OB} that precedes their switch to radial migration (17, 18). We observed changes in *Prokr2* and *PK2* expression in the OBs of coTshz1 mutant mice, and propose that TSHZ1 plays a direct role in regulation of *Prokr2* in radially migrating neuroblasts. In contrast, the strong reduction in *PK2* expression is likely a secondary consequence of the loss of granule cells in

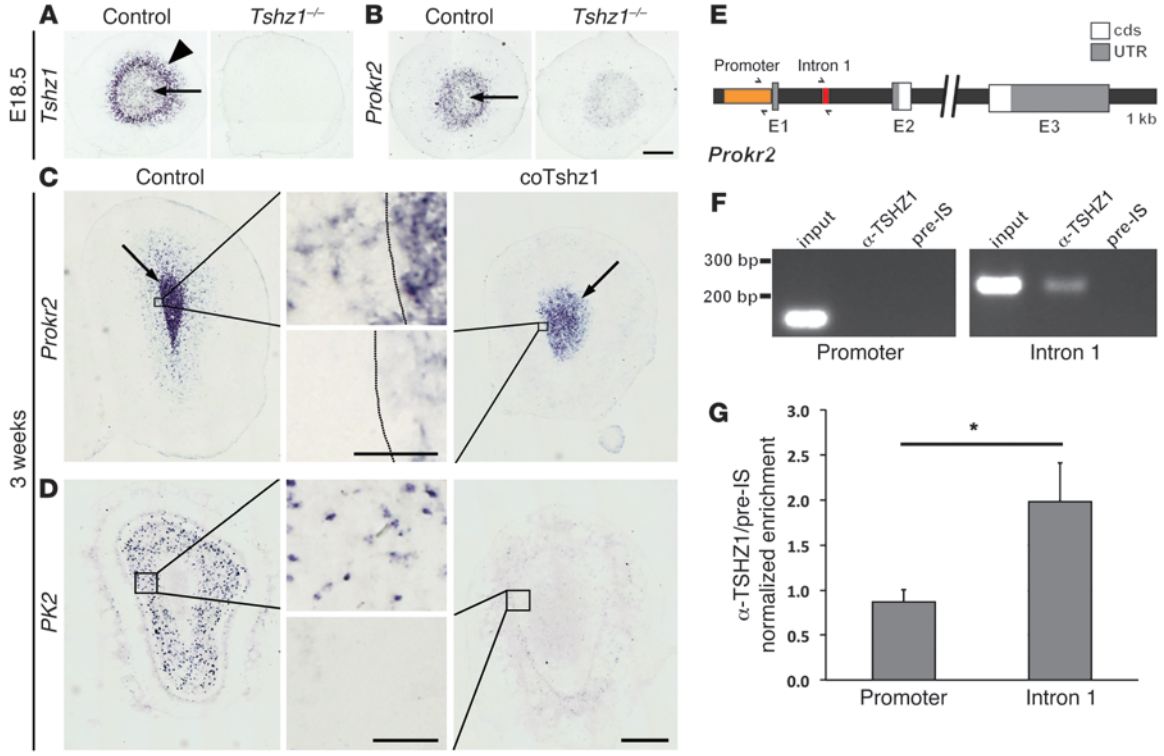

Figure 9

Tshz1 regulates expression of *Prokr2* in the OB. (**A**–**D**) Coronal sections of OBs were examined by in situ hybridization using the indicated probes. (**A**) *Tshz1* was expressed in both the RMS_{OB} (arrow) and the outer granule cell layer (arrowhead) in control mice. (**B**) *Prokr2* expression in the RMS_{OB} (arrow) was strongly reduced in *Tshz1* mutants at E18.5. (**C**) In postnatal OB, *Prokr2* was expressed in the RMS_{OB} (arrows) of controls and coTshz1 mutants, while radially migrating *Prokr2*-expressing neuroblasts were absent in the latter (insets; dotted lines denote lateral border of RMS_{OB}). (**D**) Expression of the ligand *PK2* in a subpopulation of granule cells was severely reduced in coTshz1 mutants. (**E**) *Prokr2* gene. The positions of primers flanking the putative TSHZ1 binding site in intron 1 (red) and a site in the promoter region (orange) that served as a negative control for PCR after ChIP are denoted by arrows. Exons 1–3 (E1–E3), including the coding sequences (cds; white) or 5′- and 3′-untranslated regions (UTR; gray), are also shown. (**F**) Anti-TSHZ1 or preimmune serum (pre-IS) were used in ChIP of OB tissue, and interactions were tested using conventional PCR with primer pairs in the promoter region or intron 1. (**G**) Quantitative PCR after anti-TSHZ1 ChIP, normalized to levels with preimmune serum, revealed significant enrichment for binding of TSHZ1 to intron 1 of *Prokr2*. **P* = 0.018. Scale bars: 500 μm (**C** and **D**), 200 μm (**A** and **B**), 50 μm (**C** and **D**, insets).

these animals. Although initiation of *Prokr2* expression in tangentially migrating neuroblasts of the SVZ and along the RMS prior to the OB was unaffected in coTshz1 mutant mice, maintenance of *Prokr2* expression in the RMS_{OB} was impaired, and *Prokr2*-expressing cells outside the RMS_{OB} were absent in these animals. In order to address a direct role of TSHZ1 in regulation of *Prokr2* expression, we conducted ChIP experiments on OB tissue. Although such experiments rely on detecting TSHZ1-*Prokr2* complexes that may be restricted to the small proportion of OB tissue containing radially migrating neuroblasts, we found significant enrichment of the first intron of *Prokr2* in the ChIP immunoprecipitate isolated with anti-TSHZ1 antibodies. Future studies will address the importance of this interaction in regulation of *Prokr2* expression.

We used a *Gfp* cassette in the *Tshz1* locus to mark mutant cells and serve as a reporter of transcriptional activity. We observed upregulation of GFP protein and mRNA in coTshz1 mutant mice within the RMS and RMS_{OB}, which suggests that TSHZ1 acts as an autorepressor at these sites. TSHZ1 levels might have to be tightly controlled in the RMS and RMS_{OB} to prevent precocious radial migration out of the RMS into other brain regions. Upon reaching the OB, radially migrating neuroblasts could require increased TSHZ1 levels in order to migrate out of the RMS_{OB}, probably via maintenance of *Prokr2* expression. The high levels of TSHZ1 seen within granule cells, and the failure to generate these neurons in the absence of the factor, would favor a model whereby maintenance of TSHZ1 expression is also required for neuronal differentiation once neuroblasts have migrated out of the RMS_{OB} and reached the granule cell layer.

Matsumoto et al. showed abnormal development not just of the OB, but also of the gonads and associated reproductive tracts, in mice lacking *Prokr2* (16). Furthermore, recent studies showed that human mutations in *PROKR2* or *PK2* result in Kallmann syndrome, characterized not only by defective OB development and anosmia, but also by hypogonadism (19, 20, 44, 45). This phenotype relates to a role of prokineticin signaling in the development of hypothalamic gonadotrophin-releasing hormone (GnRH) neurons, which originate in the olfactory placode and migrate to the hypothalamus. We failed to obtain litters from coTshz1 mutant female and male mice, which suggests that fertility and/or sexual behavior are affected in these animals. The *nestin-cre* transgene is expressed within a minor population of cells in the olfactory epithelium (46), which, like GnRH neurons, derive from the olfactory placode.

Whether *nestin-cre* targets GnRH neurons sufficiently early in their development remains unclear; a proper functional assessment of the role of *Tshz1* in GnRH neuron development will require future work using more suitable *cre* drivers. However, our data showing the importance of TSHZ1 in regulating *Prokr2* expression in vivo suggests that it may be a contributing factor to the development of Kallmann syndrome in humans.

Methods

Mice. See Supplemental Methods for detailed information about generation of mice carrying the $Tshz1^{GFP}$ and $Tshz1^{flox}$ alleles.

In situ hybridization, histology, and immunohistology. Single and double in situ hybridization and immunohistological analyses were performed as previously described (47). See Supplemental Methods for details.

Pulse-chase experiments with BrdU. BrdU was injected into postnatal coTshz1 mutants and control littermates at a dosage of 50 μg/g body weight. Brains were harvested 2 hours, 1 week, or 2 weeks after pulsing with BrdU, then processed for preparation of frozen sections. After staining for primary antigens, sections were postfixed in 4% PFA/phosphate buffer for 15 minutes at room temperature. DNA was then denatured by incubation in 2.4 M HCl for 10–15 minutes at 37°C. After extensive washing, immunohistology with anti-BrdU antibodies was performed (see Supplemental Methods).

Microarray analysis. Microarray analysis was initially performed on OB tissue from E18.5 $Tshz1^{GFP/+}$ (control) and $Tshz1^{GFP/\Delta}$ embryos prior to establishment of a coTshz1 mutant colony (*nestin-cre;*$Tshz1^{GFP/flox}$ conditional mutant). We found the phenotype in the OB of $Tshz1^{-/-}$ and coTshz1 mutants at E18.5 to be identical (Supplemental Figure 1). Subsequently, OB tissue from P30 *nestin-cre;*$Tshz1^{flox/+}$ (control) and coTshz1 animals was isolated. OB tissue samples were homogenized in TRIzol, and total RNA extraction was performed according to the manufacturer's instructions. 1.125 μg cRNA from each sample (n = 8 biological replicates per genotype) was hybridized to Illumina MouseRef-8 version 2.0 arrays, after labeling using the Illumina TotalPrep RNA amplification kit. Arrays were quantile normalized on probe level without background correction using Illumina Genome Studio software version 2011.1, with gene expression module version 1.9.0. Subsequently, data were $\log_2$-transformed after an offset addition of +16. Probes failing to display a detection P value less than 0.05 in all samples were discarded before performing statistical comparisons. Probes and samples were analyzed for significant differences in expression according to genotype using an ANOVA algorithm, followed by a false discovery rate (FDR) multiple-testing correction (48). ANOVA was performed for adult and embryo samples separately by controlling for the "slide" cofactor. Probes with FDR <0.1 were selected as differentially expressed (n = 865 probes [P30], 92 probes [E18.5]). After selection of candidates for verification by in situ hybridization or immunohistology, standardized mean values of 37 differentially expressed probes (representing 31 genes) were clustered using hierarchical average linkage clustering. Microarray data were deposited in GEO (accession no. GSE51761).

Mouse behavioral tests. To determine whether coTshz1 mutant mice had an impaired sense of smell, we performed several olfactory tests: (a) the buried food test, which measures the ability of mice to locate familiar food hidden underneath bedding (49); (b) the preference test, designed to identify abilities to sense attractive or aversive odors (50, 51); (c) the habituation/dishabituation test, to determine an animal's ability to habituate to different odors; and (d) the threshold test, using different concentrations of the odor TMT (51). See Supplemental Methods for details.

Olfactory testing of human subjects. Olfactory testing was performed in 5 individuals heterozygous for loss-of-function *TSHZ1* mutations, previously described by Feenstra et al. (15), and 5 controls matched for age and sex. Testing was performed using the Sniffin' Sticks test kit (Burghart Instruments; ref. 28), which is divided into 3 subtests. Odor sensitivity was tested using a 3-alternative, forced-choice task and a staircase paradigm using triplets of odor sticks, 1 with *n*-butanol and 2 blanks for each dilution step. Odor discrimination was tested using a 3-alternative forced-choice task and 16 triplets of odor sticks, with 2 containing the same odor and 1 containing a different odor. Odor identification was tested using a 4-alternative, forced-choice task with a list of 4 descriptions for each of 16 odor sticks with different odors. To determine whether the results of the control group differed significantly from those of the mutant group, unpaired t test was used. The hyposmic scores on the identification test in both control and mutant groups can be explained by the age of the participants: 6 of the individuals tested were children and were not familiar with all odors. All tests were performed by a single trained examiner.

ChIP. Chromatin was extracted from adult mouse OBs, followed by immunoprecipitation using anti-TSHZ1 antiserum or serum before immunization (preimmune serum) as a negative control. ChIP was performed as previously described (52), with minor changes. Briefly, OBs of control and mutant mice were dissociated and cross-linked with 1% formaldehyde for 15 minutes at room temperature. Chromatin was released using SDS lysis buffer during 25 cycles of sonication (30 s on, 30 s off), and the size of DNA in the chromatin fragments was checked by gel electrophoresis (Supplemental Figure 8E). Chromatin samples were then split, and DNA-protein complexes were immunoprecipitated with either anti-TSHZ1 antiserum or preimmune serum using protein A–coupled beads. After RNase and protease treatment of chromatin, reverse cross-linking was performed, followed by DNA purification using phenol-chloroform extraction and ethanol precipitation. Conventional PCR was used to test for ChIP enrichment using primers amplifying different segments covering a region 1.5 kb upstream of exon 1 and in intron 1. We showed results for 2 sets of primers: promoter (5′-CACACTCCAACTCTGCACACTTAGT-3′ and 5′-CGGAAGTCTGAGACCCTAATTCAGT-3′; 154 bp), which served as a negative control for binding in the promoter sequence, and intron 1 (5′-TTCAGGGCCATTTCAAGCACGGCTA-3′ and 5′-ACTGTCTGAGGCCAGAAGAGGGTAT-3′; 236 bp), which served to detect a putative binding site of TSHZ1 in the first intron of *Prokr2*. Quantitative PCR using the same primers and a Sybr-Green-based kit was used to examine ChIP enrichment across a total of 5 independent tissue samples, each consisting of a pool of OBs from 4 control animals. IP enrichment was calculated as the ratio of amplified product after precipitation with anti-TSHZ1 antiserum relative to preimmune serum.

Western blot. Dissected OBs of adult mice were homogenized in lysis buffer (10 mM Tris, pH 8; 1 mM EDTA; 0.5 mM EGTA; 1% Triton-X; 0.1% SDS; 0.1% Na deoxycholate; 1× Complete Protease Inhibitor Cocktail, Roche) using a Dounce homogenizer and 5× 1-minute sonication. 30 μg protein lysate was resolved using a 10% polyacrylamide gel. Proteins were transferred to a nitrocellulose membrane (Whatman) and blocked with 5% skimmed milk powder (Merck) in PBS with 0.1% Tween20 (PBST) for 1 hour at room temperature. Primary guinea pig anti-TSHZ1 antiserum (1:10,000; see above) was incubated in blocking solution for 2 hours at room temperature. Blots were washed 3 times for 10 minutes with PBST, then incubated with HRP-conjugated antibody (1:3,000 goat anti–guinea pig; Jackson Immunoresearch). A protein band corresponding to the expected size of TSHZ1 (115 kDa) was observed in Western blotting of control OB tissue, but was absent in coTshz1 mutant animals.

Statistics. Statistical significance was assessed using unpaired, 2-tailed Student's t test. Results (mean ± SEM) were obtained using GraphPad Prism 5. P values less than 0.05 were considered significant.

Study approval. All procedures with patients were approved by, and performed in accordance with the ethical standards of, the Radboud University Nijmegen Medical Centre Ethical committee. Informed consent

was obtained from all patients and healthy volunteers in accordance with the Declaration of Helsinki. All animal experiments described herein were approved in accordance with German animal welfare regulations (LaGeSo, Berlin, Germany).

Acknowledgments

The authors thank the family members and controls for their participation in this study; Carmen Birchmeier (MDC) for support and input; Thomas Müller (MDC) for critical reading of the manuscript; Maciej Czajkowski and Jochen Welcker (MDC) for helpful discussions; Carola Griffel, Claudia Päseler, Petra Stallerow, Sven Buchert, Josephine Jahnke, and Henrike Keil (MDC) for technical assistance; the MDC transgenic and microarray units for technical support and animal husbandry; Cyril Cheret (MDC) for advice on statistical analyses of behavioral tests; and Parrish Waters (Charité) for performing behavioral tests. This work was supported by grants from the German Federal Ministry for Education and Research (BMBF, NGFN-plus, "Alzheimer Disease Integrative Genomics," PNA-01GS08127-3a, to A.N. Garratt), the German Research Council (DFG, Collaborative Research Centre SFB665, to H. Wende), and ZON MW (90700388, to R.J.E. Pennings).

Received for publication July 31, 2013, and accepted in revised form November 14, 2013.

Address correspondence to: Ronald J.E. Pennings, Radboud University Nijmegen Medical Centre, P.O. Box 9101, 6500 HB Nijmegen, The Netherlands. Phone: 31.24.3617203; Fax: 31.24.3540251; E-mail: r.pennings@kno.umcn.nl. Or to: Hagen Wende, Neuroscience Program and Cardiovascular Program, Max-Delbrück-Center for Molecular Medicine, Robert-Rössle-Strasse 10, 13125 Berlin, Germany. Phone: 49.0.6221.54.8288; Fax: 49.0.6221.54.8367; E-mail: hagen.wende@pharma.uni-heidelberg.de. Or to: Alistair N. Garratt, Institute of Cell Biology and Neurobiology, Center for Anatomy, Charité University Hospital Berlin, Charitéplatz 1, 10117 Berlin, Germany. Phone: 49.0.30.450.528278; Fax: 49.0.30.450.528902; E-mail: alistair.garratt@charite.de.

1. Doetsch F, Garcia-Verdugo JM, Alvarez-Buylla A. Cellular composition and three-dimensional organization of the subventricular germinal zone in the adult mammalian brain. *J Neurosci*. 1997;17(13):5046–5061.
2. Stenman J, Toresson H, Campbell K. Identification of two distinct progenitor populations in the lateral ganglionic eminence: implications for striatal and olfactory bulb neurogenesis. *J Neurosci*. 2003;23(1):167–174.
3. Luskin MB, Boone MS. Rate and pattern of migration of lineally-related olfactory bulb interneurons generated postnatally in the subventricular zone of the rat. *Chem Senses*. 1994;19(6):695–714.
4. Tucker ES, Polleux F, LaMantia AS. Position and time specify the migration of a pioneering population of olfactory bulb interneurons. *Dev Biol*. 2006;297(2):387–401.
5. Wichterle H, Turnbull DH, Nery S, Fishell G, Alvarez-Buylla A. In utero fate mapping reveals distinct migratory pathways and fates of neurons born in the mammalian basal forebrain. *Development*. 2001;128(19):3759–3771.
6. Marin O, Rubenstein JL. Cell migration in the forebrain. *Annu Rev Neurosci*. 2003;26:441–483.
7. Sanai N, et al. Corridors of migrating neurons in the human brain and their decline during infancy. *Nature*. 2011;478(7369):382–386.
8. Mori K, Nagao H, Yoshihara Y. The olfactory bulb: coding and processing of odor molecule information. *Science*. 1999;286(5440):711–715.
9. Caubit X, Tiveron MC, Cremer H, Fasano L. Expression patterns of the three Teashirt-related genes define specific boundaries in the developing and postnatal mouse forebrain. *J Comp Neurol*. 2005;486(1):76–88.
10. Bessa J, Gebelein B, Pichaud F, Casares F, Mann RS. Combinatorial control of Drosophila eye development by eyeless, homothorax, and teashirt. *Genes Dev*. 2002;16(18):2415–2427.
11. Fasano L, et al. The gene teashirt is required for the development of Drosophila embryonic trunk segments and encodes a protein with widely spaced zinc finger motifs. *Cell*. 1991;64(1):63–79.
12. Pan D, Rubin GM. Targeted expression of teashirt induces ectopic eyes in Drosophila. *Proc Natl Acad Sci U S A*. 1998;95(26):15508–15512.
13. Caubit X, Coré N, Boned A, Kerridge S, Djabali M, Fasano L. Vertebrate orthologues of the Drosophila region-specific patterning gene teashirt. *Mech Dev*. 2000;91(1–2):445–448.
14. Coré N, Caubit X, Metchat A, Boned A, Djabali M, Fasano L. Tshz1 is required for axial skeleton, soft palate and middle ear development in mice. *Dev Biol*. 2007;308(2):407–420.
15. Feenstra I, et al. Disruption of teashirt zinc finger homeobox 1 is associated with congenital aural atresia in humans. *Am J Hum Genet*. 2011;89(6):813–819.
16. Matsumoto S, et al. Abnormal development of the olfactory bulb and reproductive system in mice lacking prokineticin receptor PKR2. *Proc Natl Acad Sci U S A*. 2006;103(11):4140–4145.
17. Ng KL, Li JD, Cheng MY, Leslie FM, Lee AG, Zhou QY. Dependence of olfactory bulb neurogenesis on prokineticin 2 signaling. *Science*. 2005;308(5730):1923–1927.
18. Prosser HM, Bradley A, Caldwell MA. Olfactory bulb hypoplasia in Prokr2 null mice stems from defective neuronal progenitor migration and differentiation. *Eur J Neurosci*. 2007;26(12):3339–3344.
19. Dode C, et al. Kallmann syndrome: mutations in the genes encoding prokineticin-2 and prokineticin receptor-2. *PLoS Genet*. 2006;2(10):e175.
20. Sarfati J, Dodé C, Young J. Kallmann syndrome caused by mutations in the PROK2 and PROKR2 genes: pathophysiology and genotype-phenotype correlations. *Front Horm Res*. 2010;39:121–132.
21. Kim KK, Adelstein RS, Kawamoto S. Identification of neuronal nuclei (NeuN) as Fox-3, a new member of the Fox-1 gene family of splicing factors. *J Biol Chem*. 2009;284(45):31052–31061.
22. Tronche F, et al. Disruption of the glucocorticoid receptor gene in the nervous system results in reduced anxiety. *Nat Genet*. 1999;23(1):99–103.
23. Brown JP, Couillard-Despres S, Cooper-Kuhn CM, Winkler J, Aigner L, Kuhn HG. Transient expression of doublecortin during adult neurogenesis. *J Comp Neurol*. 2003;467(1):1–10.
24. Petreanu L, Alvarez-Buylla A. Maturation and death of adult-born olfactory bulb granule neurons: role of olfaction. *J Neurosci*. 2002;22(14):6106–6113.
25. Batista-Brito R, Close J, Machold R, Fishell G. The distinct temporal origins of olfactory bulb interneuron subtypes. *J Neurosci*. 2008;28(15):3966–3975.
26. Kohwi M, Osumi N, Rubenstein JL, Alvarez-Buylla A. Pax6 is required for making specific subpopulations of granule and periglomerular neurons in the olfactory bulb. *J Neurosci*. 2005;25(30):6997–7003.
27. Brill MS, et al. A dlx2- and pax6-dependent transcriptional code for periglomerular neuron specification in the adult olfactory bulb. *J Neurosci*. 2008;28(25):6439–6452.
28. Hummel T, Sekinger B, Wolf SR, Pauli E, Kobal G. 'Sniffin' sticks': olfactory performance assessed by the combined testing of odor identification, odor discrimination and olfactory threshold. *Chem Senses*. 1997;22(1):39–52.
29. Altman J. Autoradiographic and histological studies of postnatal neurogenesis. IV. Cell proliferation and migration in the anterior forebrain, with special reference to persisting neurogenesis in the olfactory bulb. *J Comp Neurol*. 1969;137(4):433–457.
30. Gage FH. Neurogenesis in the adult brain. *J Neurosci*. 2002;22(3):612–613.
31. Eriksson PS, et al. Neurogenesis in the adult human hippocampus. *Nat Med*. 1998;4(11):1313–1317.
32. Ming GL, Song H. Adult neurogenesis in the mammalian brain: significant answers and significant questions. *Neuron*. 2011;70(4):687–702.
33. Nguyen L, et al. p27kip1 independently promotes neuronal differentiation and migration in the cerebral cortex. *Genes Dev*. 2006;20(11):1511–1524.
34. Ge W, et al. Coupling of cell migration with neurogenesis by proneural bHLH factors. *Proc Natl Acad Sci U S A*. 2006;103(5):1319–1324.
35. Belvindrah R, Nissant A, Lledo PM. Abnormal neuronal migration changes the fate of developing neurons in the postnatal olfactory bulb. *J Neurosci*. 2011;31(20):7551–7562.
36. Hummel T, Smitka M, Puschmann S, Gerber JC, Schaal B, Buschhuter D. Correlation between olfactory bulb volume and olfactory function in children and adolescents. *Exp Brain Res*. 2011;214(2):285–291.
37. Negoias S, et al. Reduced olfactory bulb volume and olfactory sensitivity in patients with acute major depression. *Neuroscience*. 2010;169(1):415–421.
38. Abraham NM, et al. Synaptic inhibition in the olfactory bulb accelerates odor discrimination in mice. *Neuron*. 2010;65(3):399–411.
39. Gheusi G, Cremer H, McLean H, Chazal G, Vincent JD, Lledo PM. Importance of newly generated neurons in the adult olfactory bulb for odor discrimination. *Proc Natl Acad Sci U S A*. 2000;97(4):1823–1828.
40. Krude H, et al. Choreoathetosis, hypothyroidism, and pulmonary alterations due to human NKX2-1 haploinsufficiency. *J Clin Invest*. 2002;109(4):475–480.
41. Kimura S, Hara Y, Pineau T, Fernandez-Salguero P, Fox CH, Ward JM, Gonzalez FJ. The T/ebp null mouse: thyroid-specific enhancer-binding protein is essential for the organogenesis of the thyroid, lung, ventral forebrain, and pituitary. *Genes Dev*. 1996;10(1):60–69.
42. Hu WP, Zhang C, Li JD, Luo ZD, Amadesi S, Bunnett N, Zhou QY. Impaired pain sensation in mice lacking prokineticin 2. *Mol Pain*. 2006;235.
43. Li JD, Hu WP, Zhou QY. The circadian output signals from the suprachiasmatic nuclei. *Prog Brain*

Res. 2012;199:119–127.
44. Avbelj Stefanija M, et al. An ancient founder mutation in PROKR2 impairs human reproduction. *Hum Mol Genet*. 2012;21(19):4314–4324.
45. Dode C, Rondard P. PROK2/PROKR2 Signaling and Kallmann Syndrome. *Front Endocrinol (Lausanne)*. 2013;419.
46. Murdoch B, Roskams AJ. A novel embryonic nestin-expressing radial glia-like progenitor gives rise to zonally restricted olfactory and vomeronasal neurons. *J Neurosci*. 2008;28(16):4271–4282.
47. Watakabe A, et al. Comparative analysis of layer-specific genes in Mammalian neocortex. *Cereb Cortex*. 2007;17(8):1918–1933.
48. Benjamini Y, Hochberg Y. Controlling the false discovery rate: a practical and powerful approach to multiple testing. *J R Statist Soc B*. 1995;57(1):289–300.
49. Yang M, Crawley JN. Simple behavioral assessment of mouse olfaction. *Curr Protoc Neurosci*. 2009;Chapter 8:Unit 8.24.
50. Witt RM, Galligan MM, Despinoy JR, Segal R. Olfactory behavioral testing in the adult mouse. *J Vis Exp*. 2009;(23)pii:949.
51. Kobayakawa K, et al. Innate versus learned odour processing in the mouse olfactory bulb. *Nature*. 2007;450(7169):503–508.
52. Sandmann T, Girardot C, Brehme M, Tongprasit W, Stolc V, Furlong EE. A core transcriptional network for early mesoderm development in Drosophila melanogaster. *Genes Dev*. 2007;21(4):436–449.